PCCP

COMMUNICATION

View Article Online
View Journal

Cite this: DOI: 10.1039/d6cp01323f

Received 9th April 2026,
Accepted 26th May 2026

DOI: 10.1039/d6cp01323f

rsc.li/pccp

Fluorination switches CO–arene binding to a π-hole regime, enabling nonclassical carbonyl behaviour

Imanol Usabiaga, †[a] Weixing Li, ‡[a] Camilla Calabrese, §[a] Ahmet Altun, [b] Assimo Maris, [a] Sonia Melandri, [a] Giovanni Bistoni *[c] and Luca Evangelisti *[a]

Rotational spectroscopy reveals that fluorination switches CO–arene interactions to a nonclassical lp···π-hole binding motif. CO binds perpendicularly to perfluorinated aromatics, with C ← O bond contraction analogous to metal carbonyls, highlighting how π-hole interactions control ligand behaviour in weakly bound systems.

Noncovalent interactions (NCIs) are key determinants of molecular structure and function, governing processes ranging from supramolecular assembly to catalysis and biomolecular recognition. While individually weak, their collective effects can profoundly modulate the architecture and physicochemical properties of molecular systems.[1,2]

Carbon monoxide (CO) is a paradigmatic ligand in chemistry.[3] In transition-metal complexes, its bonding is described by the interplay of σ-donation and π-backdonation, which directly affects the C–O bond length and vibrational properties. In contrast, the behaviour of CO in purely noncovalent environments remains far less understood, particularly in interactions with aromatic systems, despite the increasing relevance of π-driven NCIs in chemistry and biology.

Aromatic rings provide versatile platforms for NCIs, whose topology can be tuned by substitution. Benzene typically interacts through its electron-rich π-cloud, forming O–H···π and N–H···π interactions.[4,5] Fluorination dramatically alters this picture by reversing the electrostatic potential at the ring centre and generating a π-hole. Consequently, perfluorinated aromatics such as C_6F_6 preferentially engage in lone pair···π interactions.[6,7]

The nature of the interacting partner is equally critical. CO exhibits unusual electronic properties, including a small dipole moment and pronounced quadrupolar character, leading to interaction patterns that are difficult to predict. Previous studies have shown that CO binds above benzene with its axis nearly parallel to the ring plane.[8] Whether fluorination can induce qualitatively different binding regimes remains an open question. Here, we address this issue by combining rotational spectroscopy and high-level quantum chemical calculations, showing that fluorination switches CO binding from a π-driven to a π-hole-driven regime.

The rotational spectrum of the C_6F_6···CO complex was recorded in the 6–18 GHz range using a pulsed-jet Fourier transform microwave spectrometer.[9] The experimental details and the measured transitions are available in the SI. The observed spectrum corresponds to a symmetric top rotor, indicating that CO is oriented perpendicular to the aromatic plane. The measurements have been extended to a total of 64 transitions with several $J + 1 \leftarrow J$ progressions, with the rotational quantum number J ranging from 5 to 13. All the rotational transitions belonging to the molecular system were fitted to the following expression suited for a symmetric top: $\nu(J + 1, K \leftarrow J, K) = 2B(J + 1) - 4D_J(J + 3)^3 - 2D_{JK}(J + 1)K^2$, where B is the rotational constant, and D_J and D_{JK} are the centrifugal distortion constants. The resulting spectroscopic parameters are reported in Table 1.

Assuming unchanged monomer geometries, the distance between the centres of mass (R_{cm}) can be derived from the experimental B constant, constraining the system to a pseudo-diatomic geometry.

Using literature parameters for C_6F_6 and CO,[10,11] we estimate an intermolecular distance of R_{cm} = 3.95 Å. This value should be regarded as an approximate structural estimate

[a] Department of Chemistry G. Ciamician, University of Bologna, Via Gobetti 85, 40129, Bologna, Italy. E-mail: luca.evangelisti6@unibo.it
[b] Max-Planck-Institut für Kohlenforschung, Kaiser-Wilhelm-Platz 1, D-45470, Mülheim an der Ruhr, Germany
[c] Department of Chemistry, Biology, and Biotechnology, University of Perugia, 06123, Perugia, Italy. E-mail: giovanni.bistoni@unipg.it
† Present address: Department of Physical Chemistry, Faculty of Science and Technology, University of the Basque Country (EHU), Campus de Leioa, Ap. 644, 48080 Bilbao, Spain.
‡ Present address: Department of Chemistry, State Key Laboratory of Porous Materials for Separation and Conversion, Shanghai Key Laboratory of Molecular Catalysis and Innovative Materials, Fudan University, Shanghai 200438, China.
§ Present address: Departamento de Química Física y Química Inorgánica, Facultad de Ciencias – I.U. CINQUIMA, Paseo de Belén, 7, 47011 Valladolid, Spain.

Table 1 Experimental spectroscopic parameters of the observed $C_6F_6\cdots CO$ conformer

	$C_6F_6\cdots CO$
B/MHz	574.86208(2)[a]
D_J/kHz	0.1695(1)
D_{JK}/kHz	2.0757(3)
N[b]	64
σ[c]/kHz	1

[a] Standard error in parentheses, in units of the last digit. [b] Number of lines in the fit. [c] Root-mean-square deviation of the fit.

rather than a precise experimental determination. For comparison, in the non-fluorinated analogue ($C_6H_6\cdots CO$), CO also binds above the ring but with its axis nearly parallel to the aromatic plane. In that case, a high-resolution isotopic rotational analysis yielded R_{cm} = 3.440(3) Å.[8] Within the pseudo-diatomic approximation developed for weakly bound complexes by Millen,[12] the intermolecular stretching force constant is estimated as k_s = 3.09 N m^{-1} using:

$$k_s = \frac{16\pi^2\mu B^4}{D_J}\left(1 - \frac{B}{B_{C_6F_6}} - \frac{B}{B_{CO}}\right)$$

where μ is the pseudo-diatomic reduced mass, B and D_J are the experimental spectroscopic constants of the complex (Table 1) and $B_{C_6F_6}$ = 1029.74 MHz and B_{CO} = 57635.9687 MHz are the rotational constants of the monomers. This corresponds to a harmonic stretching frequency of 46 cm^{-1}, in good agreement with the value obtained from harmonic quantum-chemical analysis (about 60 cm^{-1}, see the SI). Assuming a Lennard-Jones-type potential, the dissociation energy is estimated as E_D = 1/72 k_s R_{CM}^2, yielding E_D = 4.0 kJ mol^{-1} (reasonably consistent with the interaction energies obtained from DFT and DLPNO-CCSD(T)/CBS calculations reported in the SI), lower than that of $C_6F_6\cdots H_2O$, E_D = 6.2 kJ mol^{-1}. These results raise key questions: what is the nature of the interaction, what determines the orientation of CO, and why does fluorination induce such a different binding topology? Given the central role of CO as a ligand, understanding its noncovalent behaviour is essential. Notably, while classical metal carbonyls exhibit C–O bond elongation, nonclassical complexes show bond contraction, providing a useful framework to interpret the present system. To interpret the origin of this binding behaviour, we analyse the electrostatic properties of the interacting partners.

To rationalize the observed behaviour, we analyse the molecular electrostatic potentials (MEPs) of benzene and its fluorinated analogue (Fig. 1). Benzene exhibits a relatively isotropic MEP, resulting in a limited electrostatic contribution to its interaction with neutral ligands. In contrast, fluorination reverses the electrostatic potential at the ring centre, generating a positive π-hole, while the fluorine atoms remain slightly negative. As a result, interactions in perfluorinated systems are dominated by electrostatics and polarization. This dual binding character of arenes becomes particularly relevant for weakly bound systems such as CO. Indeed, CO displays unusual electronic properties, with a small dipole moment (positive at O and negative at C) and a pronounced quadrupolar character. Its MEP is characterized by

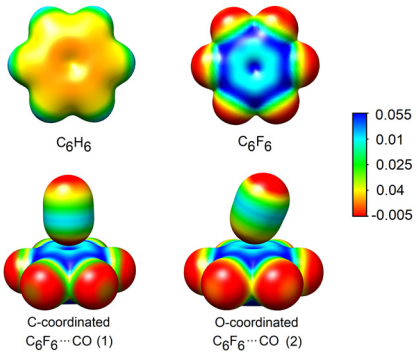

Fig. 1 On the 0.004 e Bohr^{-3} electron density isosurface calculated at the B3LYP/def2-TZVP level, (top) molecular electrostatic potential for the isolated aromatic rings, and (bottom) the superimposed molecular electrostatic potentials of the isolated fluorinated ring and CO at the adduct geometries. The color bar is given between −0.005 Eh e^{-1} (red) and +0.055 E_h e^{-1} (blue). Surfaces were rendered using UCSF Chimera.

negative regions at both termini, slightly more pronounced on carbon, and a positive electrostatic potential along the cylindrical surface of the bond (Fig. S3). Consequently, CO behaves as a quadrupole-dominated molecule, leading to interaction patterns that are not readily captured by simple dipole-based models.[13]

While MEP analysis provides qualitative insight into possible binding orientations, a quantitative description requires full quantum chemical calculations. Exploration of the conformational space of the arene$\cdots$CO complexes at the B3LYP-D3(BJ)/def2-TZVP level of theory[14–16] using ORCA[17–19] yields the structures shown in Fig. 2, with computed spectroscopic parameters reported in the SI. The relative stability of these conformers is strongly method-dependent. The Hartree–Fock method fails to reproduce the correct energetic ordering, while MP2 significantly overestimates energy differences. Accurate treatment of dynamic electron correlation is therefore essential, and DLPNO-CCSD(T) calculations are required to reliably reproduce the experimental trends.[20,21] Notably, B3LYP-D3 relative energies closely match the DLPNO-CCSD(T) results for both fluorinated and non-fluorinated systems, supporting its use for structural and energetic analysis. The corresponding thermochemical contributions to the interaction energies are reported in Table S2.

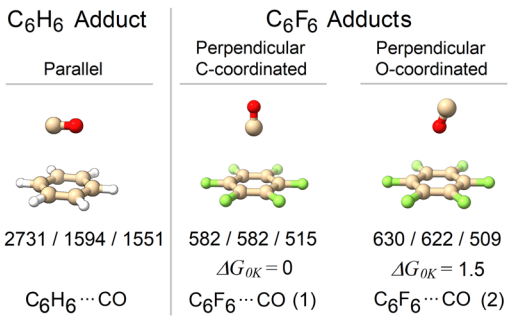

Fig. 2 Adducts of fluorinated and non-fluorinated benzene with CO together with rotational $A/B/C$ constants (MHz) calculated at the B3LYP-D3(BJ)/def2-TZVP level and ΔG_{0K} (kJ mol^{-1}) calculated at the DLPNO-CCSD(T)/CBS level.

Among the identified structures, the perpendicular C-bound conformer is found to be the most stable and is fully consistent with the experimental rotational constants.

In the $C_6H_6\cdots CO$ complex, CO is located above the benzene ring with its molecular axis nearly parallel to the aromatic plane (Fig. 2). In contrast, the $C_6F_6\cdots CO$ complex features two perpendicular conformers, corresponding to C-coordinated ($C_6F_6\cdots CO$ (1)) and O-coordinated ($C_6F_6\cdots CO$ (2)) arrangements. Calculations identify $C_6F_6\cdots CO$ (1) as the most stable structure at 0 K, and only this conformer reproduces the experimental rotational B constant (Table 1 and Fig. 3).

The relative free energies of the fluorinated adducts (Table 2), referenced to the most stable conformer $C_6F_6\cdots CO$ (1), were analysed using local energy decomposition (LED).[22–26] In this framework, the free energy difference is partitioned as $\Delta G = \Delta G_{corr} + \Delta E_{disp} + \Delta E_{no\text{-}disp}$ where ΔG_{corr} accounts for thermal and entropic contributions (or zero-point energy at 0 K), while ΔE_{disp} and $\Delta E_{no\text{–}disp}$ represent the dispersive (London dispersion) and non-dispersive (electrostatics and polarization) components, respectively. This decomposition enables quantitative assessment of the different physical contributions governing the interaction. The analysis shows that C-coordination is consistently favoured by both dispersive and non-dispersive terms, whereas entropy slightly stabilizes the O-bound conformer. This competition accounts for the predicted inversion of stability at higher temperatures, while remaining consistent with the low-temperature experimental conditions. To visualize the role of dispersion, dispersion interaction density (DID) plots (Fig. 4) were computed at the DLPNO-CCSD level within the LED framework,[23,27] providing a spatial representation of London dispersion contributions. These results confirm that dispersion contributes significantly to the stabilization of both conformers, although it does not determine their relative ordering.

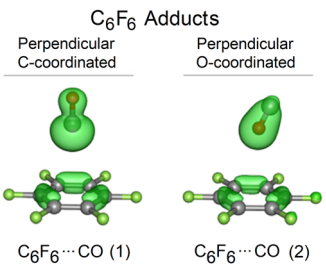

Fig. 3 DLPNO-CCSD/LED dispersion interaction density (DID) plots of fluorinated adducts with an isosurface contour value of 0.01 kcal mol^{-1} Bohr^{-3}.

Table 2 Local energy decomposition of the relative conformational energy (kJ mol^{-1}) for the interaction of CO with the fluorinated aromatic compounds

	ΔG_{298K}	ΔG_{0K}	ΔE	ΔE_{disp}	$\Delta E_{no\text{-}disp}$
$C_6F_6\cdots CO$ (1)[a]	0.0	0.0	0.0	0.0	0.0
$C_6F_6\cdots CO$ (2)	−0.5	1.5	1.9	0.8	1.1

[a] Reference binding energy contributions: ΔE_{bind} = −6.9 kJ mol^{-1}, E_{disp} = −11.3 kJ mol^{-1}, and $\Delta E_{no\text{-}disp}$ = 4.4 kJ mol^{-1}.

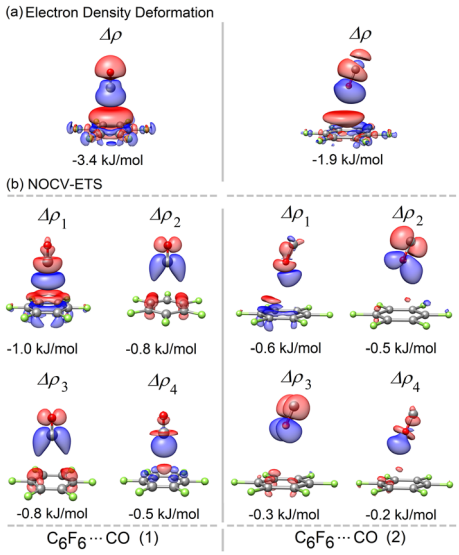

Fig. 4 (a) One-electron deformation density of orbital relaxation at the B3LYP-D3(BJ)/def2-TZVP level and (b) its largest decomposed NOCV-ETS binding modes for $C_6F_6\cdots CO$ (1) (left) and $C_6F_6\cdots CO$ (2) (right) with the corresponding energy contributions (isosurface contour value: 8×10^{-5} e Bohr^{-3}). Blue and red electron density surfaces identify regions of electron density accumulation and depletion, respectively.

To further elucidate the origin of the interaction, NOCV-ETS analysis[23,28] was performed at the B3LYP-D3 level. The decomposition reveals that the interaction in the fluorinated system is dominated by a lp$\cdots\pi$-hole motif, in which both σ and π orbitals of CO are polarized towards the electron-deficient region at the centre of the aromatic ring. This results in a pronounced accumulation of electron density in the intermolecular region and a net polarization of the C–O bond in the C ← O direction, as evidenced by the deformation density maps (Fig. 4).

This polarization is reflected in theoretically predicted structural changes. In the fluorinated complex, the C–O bond is shortened with respect to the isolated molecule (by ∼0.4 mÅ), whereas in the non-fluorinated $C_6H_6\cdots CO$ complex, a slight elongation is observed (by ∼0.6 mÅ). At the same time, the experimental intermolecular distance increases upon fluorination (R_{cm} = 3.95 Å *vs.* 3.44 Å in $C_6H_6\cdots CO$), highlighting the different balance of attractive interactions in the two systems. The behaviour of the non-fluorinated complex is consistent with a "classical" Dewar–Chatt–Duncanson-type picture,[3] where σ-donation from CO is accompanied by a weak π-backdonation from the aromatic π-system, leading to a modest elongation of the C–O bond. In contrast, the fluorinated system exhibits a nonclassical regime, where π-backdonation is strongly reduced and electrostatic polarization dominates, resulting in bond contraction. Such behaviour closely parallels that observed in carbonyl complexes of cationic metals, where a reduced electron density at the metal centre limits π-backdonation and favours shortening of the C–O bond. In this context, the π-hole of the fluorinated aromatic ring acts as an electrostatic analogue of a positively charged metal centre. It should be noted, however, that the magnitude of the structural response is markedly different: while metal–carbonyl bond distances typically vary on the mÅ scale, the corresponding

changes in weakly bound aromatic systems occur on a significantly smaller (sub-mÅ) scale, reflecting the fundamentally different strength of the interactions involved.[29] The balance between electrostatic polarization and π-backdonation therefore governs the C–O bond response, with elongation occurring in electron-rich environments and contraction in electron-deficient ones.

In summary, we demonstrate that fluorination fundamentally alters the binding topology of CO to aromatic systems by replacing interaction with the electron-rich π-cloud of benzene with binding to the positive π-hole region of C_6F_6. Rotational spectroscopy provides direct structural evidence of a perpendicular binding motif, while quantum chemical analysis reveals a lp···π-hole interaction that strongly polarizes the CO molecule. This interaction induces a contraction of the C–O bond, mimicking nonclassical carbonyl behaviour typically associated with cationic metal centres, despite the absence of a metal. These findings establish π-hole interactions as a mechanism to control ligand-like properties in weakly bound systems, providing a conceptual bridge between noncovalent interactions and coordination chemistry.

More broadly, this work highlights how subtle electronic tuning can induce qualitatively different bonding regimes, opening new perspectives for the design of supramolecular systems and functional materials.

Conflicts of interest

There are no conflicts to declare.

Data availability

The data supporting this article have been included as part of the supplementary information (SI). Data supporting the findings of this study are openly available in the University of Bologna repository at https://amsacta.unibo.it/id/eprint/8959/. Supplementary information is available. See DOI: https://doi.org/10.1039/d6cp01323f.

Acknowledgements

We acknowledge the CINECA award under the ISCRA initiative for the availability of high-performance computing resources and support. C. C. thanks the Spanish Ministerio de Ciencia e Innovación and the European Regional Development Fund (MICINN–ERDF) for funding support through the project PID2022-136525NA-I00. We acknowledge the project PRIN2022 (MUR code 2022WKTH9E and CUP J53D23008810006) funded by the European Union – Next Generation EU.

References

1 K. Müller-Dethlefs and P. Hobza, *Chem. Rev.*, 2000, **100**, 143.
2 E. R. Johnson, S. Keinan, P. Mori-Sánchez, J. Contreras-García, A. J. Cohen and W. Yang, *J. Am. Chem. Soc.*, 2010, **132**, 6498.
3 G. Frenking, I. Fernández, N. Holzmann, S. Pan, I. Krossing and M. Zhou, *JACS Au*, 2021, **1**, 623.
4 P. Halder, M. S. Krishnan and E. Arunan, *J. Mol. Spectrosc.*, 2020, **370**, 111277.
5 D. A. Rodham, S. Suzuki, R. D. Suenram, F. J. Lovas, S. Dasgupta, W. A. Goddard III and G. A. Blake, *Nature*, 1993, **362**, 735.
6 L. Evangelisti, K. Brendel, H. Mäder, W. Caminati and S. Melandri, *Angew. Chem., Int. Ed.*, 2017, **56**, 13699.
7 W. Li, I. Usabiaga, C. Calabrese, L. Evangelisti, A. Maris, L. B. Favero and S. Melandri, *Phys. Chem. Chem. Phys.*, 2021, **23**, 9121.
8 T. Brupbacher and A. Bauder, *J. Chem. Phys.*, 1993, **99**, 9394.
9 W. Caminati, L. Evangelisti, G. Feng, B. M. Giuliano, Q. Gou, S. Melandri and J. U. Grabow, *Phys. Chem. Chem. Phys.*, 2016, **18**, 17851.
10 T. S. Den, H. M. Frey and S. Leutwyler, *J. Chem. Phys.*, 2014, **141**, 194303.
11 F. J. Lovas and P. H. Krupenie, *J. Phys. Chem. Ref. Data*, 1974, **3**, 245.
12 D. J. Millen, *Can. J. Chem.*, 1985, **63**, 1477.
13 H. Kim, V. D. Doan, W. J. Cho, R. Valero, Z. Aliakbar Tehrani, J. M. L. Madridejos and K. S. Kim, *Sci. Rep.*, 2015, **5**, 1.
14 F. Weigend, *Phys. Chem. Chem. Phys.*, 2006, **8**, 1057.
15 A. D. Becke, *J. Chem. Phys.*, 1993, **98**, 5648.
16 S. Grimme, S. Ehrlich and L. Goerigk, *J. Comput. Chem.*, 2011, **32**, 1456.
17 F. Neese, *WIREs Comput. Mol. Sci.*, 2012, **2**, 73.
18 F. Neese, *WIREs Comput. Mol. Sci.*, 2018, **8**, e1327.
19 F. Neese, *WIREs Comput. Mol. Sci.*, 2022, **12**, e1606.
20 C. Riplinger, P. Pinski, U. Becker, E. F. Valeev and F. Neese, *J. Chem. Phys.*, 2016, **144**, 24109.
21 F. Neese, A. Hansen and D. G. Liakos, *J. Chem. Phys.*, 2009, **131**, 64103.
22 W. B. Schneider, G. Bistoni, M. Sparta, M. Saitow, C. Riplinger, A. A. Auer and F. Neese, *J. Chem. Theory Comput.*, 2016, **12**, 4778.
23 A. Altun, F. Neese and G. Bistoni, *J. Chem. Theory Comput.*, 2019, **15**, 215.
24 A. Altun, M. Saitow, F. Neese and G. Bistoni, *J. Chem. Theory Comput.*, 2019, **15**, 1616.
25 G. Bistoni, *WIREs Comput. Mol. Sci.*, 2020, **10**, e1442.
26 A. Altun, R. Izsák and G. Bistoni, *Int. J. Quantum Chem.*, 2021, **121**, e26339.
27 A. Wuttke and R. A. Mata, *J. Comput. Chem.*, 2017, **38**, 15.
28 M. P. Mitoraj, A. Michalak and T. Ziegler, *J. Chem. Theory Comput.*, 2009, **5**, 962.
29 G. Bistoni, S. Rampino, N. Scafuri, G. Ciancaleoni, D. Zuccaccia, L. Belpassi and F. Tarantelli, *Chem. Sci.*, 2016, **7**, 1174.